ELSEVIER

Biophysical Chemistry 90 (2001) 123–133

Biophysical Chemistry

www.elsevier.nl/locate/bpc

Rotational dynamics of surface probes in lipid vesicles

M.M.G. Krishna[1], Arvind Srivastava[2], N. Periasamy*

Department of Chemical Sciences, Tata Institute of Fundamental Research, Homi Bhabha Road, Colaba, Mumbai 400 005, India

Received 28 August 2000; received in revised form 9 January 2001; accepted 10 January 2001

Abstract

Translational and rotational diffusion of fluorescent molecules on the surface of small biological systems such as vesicles, proteins and micelles depolarize the fluorescence. A recent study has treated the case of the translational dynamics of surface probes (M.M.G. Krishna, R. Das, N. Periasamy and R. Nityananda, J. Chem. Phys., 112 (2000) 8502-8514) using Monte Carlo and theoretical methods. Here we extend the application of the methodologies to apply the case of rotational dynamics of surface probes. The corresponding fluorescence anisotropy decays were obtained using the Monte Carlo simulation methods for the two cases: surface probes undergoing rotational dynamics on a plane and on a sphere. The results were consistent with the theoretical equations which show that Monte Carlo methods can be used to simulate the surface diffusion problems. The anisotropy decay for the rotational diffusion of a molecule on a planar surface is single exponential and the residual anisotropy is zero. However, residual anisotropy is finite for the case of rotational diffusion on a sphere because of the spatial averaging of the anisotropy function. The rotational correlation time in both the cases is $(4D_{rot})^{-1}$ with D_{rot} being the rotational diffusion coefficient. Rotational dynamics of a surface bound dye in a single giant liposome and in sonicated vesicles were studied and the results were explained according to the theoretical equations. A fast component of fluorescence depolarization was also observed for sonicated vesicles which was interpreted as wobbling-in-cylinder dynamics of the surface-bound dye.

Keywords: Monte Carlo simulation; Fluorescence anisotropy; Fluorescence microscopy; Giant vesicle; Lipid membrane; Surface diffusion; Rotational diffusion

* Corresponding author. Tel.: +91-22-215-2971/2979; fax: +91-22-215-2110/2181.
E-mail address: peri@tifr.res.in (N. Periasamy).
[1] Present address. Department of Biophysics and Biochemistry, University of Pennsylvania School of Medicine, Philadelphia, PA 19104-6059, USA. e-mail: *mmg@hxiris.med.upenn.edu*; fax: +1-215-898-2415.
[2] Present address. Department of Biochemistry and Biophysics, University of North Carolina, Chapel Hill, NC 27516-7260, USA.

0301-4622/01/$ - see front matter
PII: S0301-4622(01)00137-5

1. Introduction

Time resolved fluorescence anisotropy measurements provide important information about the dynamics in biological systems [1–3]. For this reason, the fluorescence of various extrinsic and intrinsic fluorophores is widely used in the study of biological systems. The fluorescence anisotropy decay is caused by both the dynamics of the fluorophore and the dynamics of the biological system into which the fluorophore is incorporated. The dynamics of a fluorophore in a biological system, which is microheterogeneous, is completely different from that in homogeneous liquids. In the case of liquids, the rotational diffusion does not experience any hindrance in any particular direction and hence the fluorescence anisotropy decay of most dye molecules in liquids decays to zero. The decay is a single exponential [2] and occasionally two exponentials [4,5] based on the shape and size of the fluorophore. The rotational correlation time (or reorientation time) is $(6D_{rot})^{-1}$, where D_{rot} is the rotational diffusion constant. In the case of biological systems, the situation becomes complex. The surrounding anisotropic medium restricts the rotational diffusion of the fluorophore and hence the anisotropy decay in most cases does not decay to zero at infinite time. The internal dynamics of a fluorophore is generally described in terms of various physical models, among which the most commonly used one is the wobbling-in-a-cone model [6,7]. However, when the fluorophore is bound to the surface of a biological system such as vesicles, proteins and micelles which are of nanometer size, the fluorescence depolarization dynamics are also determined by the surface diffusion of the dye on the biological surface. In spite of the numerous studies of fluorescence dynamics of fluorophores bound to membrane [7,6], proteins [8] and micelle [9–13], analytical equations are not available for the anisotropy decay due to translational and rotational diffusion for surface-bound fluorophores. These diffusion equations are also necessary for understanding biological phenomena at a molecular level where the surface diffusion of solutes bound to different surfaces directly influence the rate of metabolism or the rate at which the chemical signals are conveyed [14].

In a recent study [15,16], we used Monte Carlo procedures to simulate the translational diffusion on a spherical surface and obtained the corresponding theoretical equations. Here, we apply the same methodologies to the case of rotational dynamics of surface probes. The purpose of the Monte Carlo simulations described here and in our previous work [15,16] in the case of a spherical surface, is to obtain the same result that can be obtained from theory and to illustrate the usefulness of these simulations in simulating the diffusion processes on more complicated surfaces which cannot be treated analytically. The framework of solving the translational and rotational dynamics of a fluorophore on the surface of a spherical particle can be extended to fluorophores of different characteristics and surfaces of different shapes. Experimentally measured anisotropy decay of a surface probe in small and large vesicle membranes are interpreted in accord with these theoretical results.

Fluorescence anisotropy decay in a biological system is generally measured by two popular methods, standard cuvette based experiments or using fluorescence microscopy methods where localized information about the system under study can be obtained. It is a common practice in literature to use the same models, to describe the dynamics of the fluorophores measured using these two methods, based on the view that the dynamics of the fluorophore is completely controlled only by the biological system and does not depend on the method that is used to collect the information. However, this may not be true. As illustrated in this work on surface dynamics, the same system such as a surface probe in lipid vesicles can give rise to two different fluorescence anisotropy decays depending on how it is measured, although it is experiencing the same dynamics.

2. Methods

2.1. Monte Carlo simulations

Monte Carlo simulations were carried out to obtain the fluorescence anisotropy decay equations due to the rotational diffusion of dipoles on a spherical surface. The procedure is similar to the one described before for simulating the translational diffusion [15] and the modifications for rotational diffusion on a surface are briefly described as follows. It involves three steps: initial selection of the excited dipoles, rotational diffusion of the dipoles on the spherical surface with no translational diffusion and calculation of the anisotropy function. In this Monte Carlo simulation procedure, a random number generator ran2 (from 'Numerical recipes in C' [17]) is used to generate the random numbers.

2.1.1. Selection of the initial distribution of the point dipoles

Let R be the radius of the sphere on which the dipoles are diffusing and D_{rot} be the rotational diffusion coefficient. Let θ and ϕ be the standard polar angles of the dipole vector in the laboratory xyz frame where the z-axis is coincident with the polarization of the exciting laser pulse. Prior to the excitation by light, the ground state populations of the dipoles were selected randomly, populated across the spherical surface and oriented parallel to the membrane surface, i.e., making an angle $\alpha = 90°$ with the respective radial vectors of the sphere. For this purpose, initially the radial vectors distributed randomly over the sphere were selected. Then with a randomly oriented normal vector $\hat{N}$ to the respective radial vector, as the axis of rotation, the radial vector $\overline{R}$ is rotated through the angle of 90° using the three dimensional rotation matrix $D_{\hat{N}}(\alpha = 90°)$ [whose form is given in Section 2.1.2] to obtain the dipole vector $\hat{V}$. The selection of the random normal vector $\hat{N}$ is made as described previously [15] using the random numbers. The dipole vectors $\hat{V}$, thus chosen were excited with the probability of excitation $\cos^2\theta$. This was done using the transformation method described previously [17,15].

2.1.2. Diffusion of the dipoles on the spherical surface

The rotational diffusion of the excited dipoles on the surface was performed by rotating the dipoles through the specified angle about the respective radial vectors using the corresponding three dimensional rotation matrices. The three dimensional rotation matrix used in these simulations is given as [18,15]:

$$D_{\hat{n}}(\beta) = \begin{pmatrix} \cos\beta + (1-\cos\beta)n_1^2 & (1-\cos\beta)n_1n_2 - n_3\sin\beta & (1-\cos\beta)n_1n_3n_2 + \sin\beta \\ (1-\cos\beta)n_1n_2 + n_3\sin\beta & \cos\beta + (1-\cos\beta)n_2^2 & (1-\cos\beta)n_2n_3 - n_1\sin\beta \\ (1-\cos\beta)n_3n_1 - n_2\sin\beta & (1-\cos\beta)n_3n_2 + n_1\sin\beta & \cos\beta + (1-\cos\beta)n_3^2 \end{pmatrix} \quad (1)$$

where β is the angle of rotation and $\hat{n} = (n_1, n_2, n_3)$ represent the axis of rotation. Here β is chosen as 1° per iteration and $\hat{n}$ is just the unit vector along the respective radial vector $\overline{R}$.

2.1.3. Calculation of the anisotropy function

The fluorescence intensity along the laboratory x, y and z-axis was calculated as squares of the respective components of the dipole vector $\hat{V}$ at different times during the diffusion. From these three intensities, the anisotropy function was calculated using the appropriate equation:

$$r(t) = \frac{I_{\parallel} - I_{\perp}}{I_{\parallel} + 2I_{\perp}} \quad (2)$$

The diffusion of the dipoles was continued until the anisotropy decayed to a value which is

comparable to the accuracy ($< 0.1\%$ of the initial value) in typical fluorescence anisotropy experiments.

The decay is simulated for the two cases: (i) where all the dipoles are situated in a plane (no spherical averaging); and (ii) where all the dipoles are distributed over the entire spherical surface and the simulated anisotropy decay is the average over all the dipoles (spherical averaging). Fig. 1 illustrates the experimental examples for these two cases. As shown in the figure, the examples include: (i) the rotational diffusion of surface probes in a planar bilayer membrane (or in the case of a giant liposome) and the fluorescence anisotropy is measured for the fluorophores from a small area (diameter $\approx 1.2 \pm 0.2$ μm [19]) of the planar membrane under a fluorescence microscope (no spherical averaging) and (ii) when the fluorescence anisotropy is observed from the dye incorporated in sonicated vesicles in a cuvette where the collected fluorescence anisotropy is from the probes distributed over the entire spherical vesicle. In the first case of rotational diffusion on a plane, if the dipoles are oriented in the yz-plane, then there will not be any intensity component along the x-axis and hence $I_x = 0$ at all times. In this case, $I_{\parallel} = I_z$, $I_{\perp} = I_y$ and:

$$r(t) = \frac{I_z - I_y}{I_z + I_y} \tag{3}$$

In the second case of surface diffusion on a sphere, $I_{\parallel} = I_z$, $I_{\perp} = I_x = I_y$ and:

$$r(t) = \frac{I_z - I_x}{I_z + I_x + I_y} = \frac{I_z - I_y}{I_z + I_x + I_y} \tag{4}$$

The validity of each and every step in the above simulation procedure was checked with the help of computer graphics. The simulation was done with approximately 100 000 dipoles diffusing on a spherical surface, using a DEC Alpha OSF/1 computer system. The simulation was also carried out for varying values of radius of the sphere R and the rotational diffusion coefficient D_{rot}.

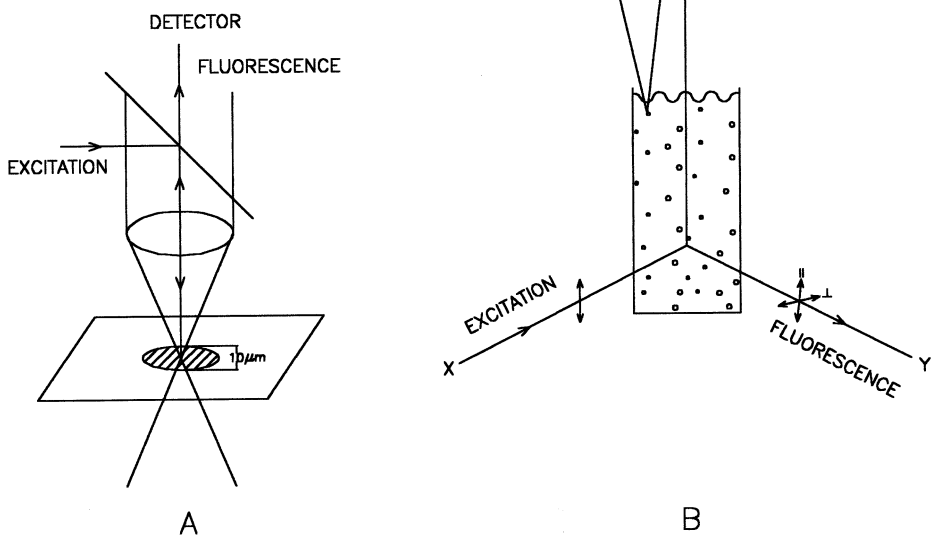

Fig. 1. The calculation of the fluorescence anisotropy in the case of a planar bilayer membrane (a) does not involve spherical averaging due to the fluorophore distribution as in the case of sonicated vesicles in a cuvette (b).

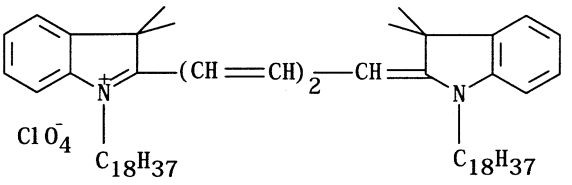

$DiIC_{18}(5)$

Fig. 2. Molecular structure of the dye $DiIC_{18}(5)$.

2.2. Experimental section

2.2.1. Materials

$DiIC_{18}(5)$ (1,1′-dioctadecyl-3,3,3′,3′-tetramethylindocarbocyanine perchlorate, Molecular Probes Inc., USA) and Egg PC (L-α-Phosphatidylcholine from fresh Egg Yolk, Sigma Chemical Co., USA) were used as received. The chemical structure of the dye is shown in Fig. 2. The fluorescence decay of the dye in ethanol is a single exponential with a lifetime of 1.24 ns indicating that the dye was of the highest purity.

The sonicated Egg PC liposomes were prepared as described earlier [20]. The sonicated vesicles are of single bilayer with diameters in the range of 200–400 Å with nearly 70% of the vesicles having diameters ≈ 300 Å. The dye was added to the vesicles and kept overnight at 4°C for equilibration. The dye (0.80 μM) to lipid (0.14 mM) ratio was 1:180. For the preparation of giant liposomes, the dye was mixed with the lipid (in the molar ratio of 1:118) in a chloroform/methanol mixture and was dried to form a thin layer. The thin layer was hydrated to form the giant liposomes [21]. The typical size of these liposomes was approximately 10 μm as calibrated using the micron size latex beads on the fluorescence microscope.

2.2.2. Fluorescence measurements

The steady state fluorescence and anisotropy measurements were made using either Shimadzu RF540 or SPEX Fluorolog 1681 T format spectrofluorophotometers. The time resolved fluorescence measurements were made using a high repetition rate (800 kHz) picosecond dye laser (rhodamine 6G) coupled with Time correlated single photon counting (TCSPC) spectrometer described elsewhere [22,23], currently using a microchannel plate photomultiplier (Hamamatsu 2809). The sample was excited with vertically polarized light and the fluorescence decay was collected with an emission polarizer kept at a magic angle (≈ 54.7°) with respect to the excitation polarizer for measuring fluorescence lifetimes. For the anisotropy measurements, the fluorescence intensities were measured with the emission polarizer set at parallel or perpendicular orientations with respect to the excitation polarizer. Geometry factor (G-factor) for the TCSPC setup was determined by using the Nile red dye solution in ethanol whose rotational correlation time (0.18 ns) is faster than its fluorescence lifetime (3.57 ns). The instrument response function (IRF) was recorded using a non-dairy creamer scattering solution. The full width at half maximum (FWHM) of IRF is approximately 200 ps. The typical peak count in the emission decay for fluorescence intensity and anisotropy measurements was approximately 10 000 and the time per channel was 37.84 ps. The samples were excited at the wavelength of 600 nm.

For the experiments with giant liposomes, an inverted epifluorescence microscope (Nikon, Diaphot 300) coupled with the above mentioned picosecond dye laser was used [19,24,25]. The $DiIC_{18}(5)$ samples were excited at the wavelength of 600 nm. The laser beam, after passing through a dichroic mirror (XF44 of Omega Optical Co., USA) was focussed onto a single giant liposome with the help of an objective lens (40 ×, NA 0.55, Nikon). The diameter of the focussed laser beam was typically approximately 1.0 μm. The fluorescence was collected by the same objective lens, passed through a 645 nm cut-off filter, a Glan-Thomson polarizer and detected by a photon counting photomultiplier (XP2020Q). The G factor was determined by using the Kiton red (Sulforhodamine B, Exciton Inc., USA) solution in water whose rotational correlation time (0.20 ns) is faster than its lifetime (1.55 ns). The instrument response function (IRF) was measured by

monitoring the fluorescence of Oxonol VI (Propyl Oxonol) in Ethanol whose fluorescence lifetime is less than 30 ps (less than one time per channel). Since Oxonol VI shows fluorescence in the wavelength region of $DiIC_{18}(5)$ and Kiton red, the same optical elements were used for collecting both the IRF and the emission profiles. The FWHM of the IRF was approximately 280 ps. Typical peak counts in the emission decay for fluorescence intensity and anisotropy measurements was approximately 10 000 and the time per channel was 43.22 ps.

The experimentally measured fluorescence decay data, whether in cuvette experiments or in microscopy experiments, is a convolution of the instrument response function with the intensity decay function. The intensity decay data were fitted to the appropriate equations by an iterative deconvolution procedure using Levenberg–Marquardt algorithm for optimization of the parameters [22,26,27]. In the case of systems studied here, the fluorescence decay data collected at the magic angle was fitted to either a single or a double exponential function as:

$$I(t) = \Sigma_i \alpha_i \exp\left(-\frac{t}{\tau_i}\right); \quad i = 1,2 \tag{5}$$

where α_i and τ_i are the amplitudes and the lifetimes. The polarized fluorescence decays (parallel and perpendicular) were fitted simultaneously [28] to obtain a single set of parameters common to both the decays as:

$$\begin{aligned} I_{\parallel} &= \tfrac{1}{3} I(t)[1 + 2r(t)] \\ I_{\perp} &= \tfrac{1}{3} I(t)[1 - r(t)] \end{aligned} \tag{6}$$

where $r(t)$ is the anisotropy function whose explicit form depends on the model under consideration. The goodness of the fits were judged by the Chi square value (1.0 ± 0.2) and the random residual distribution.

3. Results and discussion

3.1. Results of the Monte Carlo simulations

The fluorescence anisotropy decays obtained from the Monte Carlo simulations of the rotational diffusion of dipoles on the surface of a plane and on the surface of a sphere are as shown in Fig. 3. These two cases were illustrated in Fig. 1. As explained in Section 2.1, anisotropy decay in the latter case is computed by spherical averaging because of distribution of dipoles on the sphere with respect to the z-axis. From the figure, one can clearly see that the anisotropy decays to zero ($r_\infty = 0$) in the case of diffusion on a plane whereas it decays to a non-zero value ($r_\infty \neq 0$) in the case where the dipoles are undergoing rotational diffusion on the surface of a sphere.

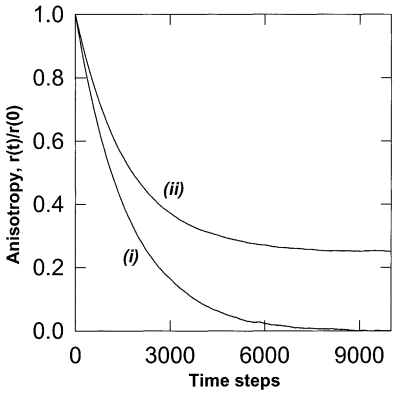

Fig. 3. Fluorescence anisotropy decays obtained from the Monte Carlo simulations of the rotational diffusion of dipoles (i) on the surface of a plane and (ii) on the surface of a sphere.

Both the fluorescence anisotropy decays are single exponential. The fluorescence anisotropy decays to one-fourth of its initial value in the case of rotational diffusion on the surface of a sphere. These results can be summarized as follows: the anisotropy decay due to rotational diffusion of the molecular dipoles on the surface is

$$\frac{r(t)}{r(0)} = c \exp(-4D_{rot}t) + (1 - c) \tag{7}$$

where $c = 1$ for the case where the anisotropy decay was simulated with the dipoles situated in a plane (no spherical averaging) and $c = \frac{3}{4}$ for the case where the dipoles are distributed over the entire sphere and the anisotropy function is calculated with spherical averaging (i.e., averaging over all the dipoles).

3.2. Theoretical derivation of the simulation results

Let θ represent the angle made by the rotating dipole with the axis of polarization of the exciting light (z-axis) as shown in Fig. 4. This angular coordinate is enough to define the position of a rotating dipole at any time t during the rotation on the plane. The diffusion equation in this case [29] becomes:

$$\frac{\partial}{\partial t}P(\theta,t) = D_{rot}\nabla^2 P(\theta,t) \tag{8}$$

where $P(\theta,t)$ is the probability of finding the dipole at the angle θ at time t, ∇^2 is the laplacian in θ. Hence Eq. (8) results in:

$$\frac{\partial^2}{\partial\theta^2}P(\theta,t) = -\frac{\lambda}{D_{rot}}P(\theta,t) \tag{9}$$

The general solution which satisfies the above differential equation is:

$$P(\theta,t) = \Sigma_l A_l \exp(\pm il\theta)\exp(-l^2 D_{rot}t) \tag{10}$$

where A_l are the appropriate scaling factors. In this case where the dipoles are located on a plane, the fluorescence anisotropy becomes:

$$r(t) = \langle \cos 2\theta \rangle_t \tag{11}$$

Using the solution (Eq. (10)), the equation for the fluorescence anisotropy is obtained as:

$$r(t) = k\exp(-4D_{rot}t) \tag{12}$$

where k is a constant. That is, the anisotropy decay due to the rotational diffusion of the dipoles on a plane is single exponential with the correlation time $(4D_{rot})^{-1}$. This is the exact result which was also obtained by the Monte Carlo simulations.

The reason for the different values of c (Eq. (7)) in the two cases where the dipoles are distributed over a planar membrane and on a sphere, can be understood as follows: in the case of a planar membrane, the initially excited anisotropic population of dipoles undergoes random rotational diffusion in the plane resulting in equal intensities along the two axes on the plane. This makes the anisotropy at infinite time, r_∞, which is $(1-c)$ in the Eq. (7) as zero; but in the case of a sphere, the initially excited population of dipoles centered about the z-axis upon random rotational diffusion and no translational diffusion, results in the intensities along the three axes in the ratio $I_z{:}I_x{:}I_y$ as 2:1:1 at infinite time. This makes the r_∞ equal to $\frac{1}{4}$ and hence c becomes $\frac{3}{4}$.

The value of c in the above equation can serve as an indicator of the curvature of the surface on which the molecules are undergoing diffusion. In the case of a plane which is of zero curvature, the c value is equal to zero whereas in the case of sphere which is a surface that is of maximum possible curvature, the c value is 0.25. For other surfaces with less curvature, its value will be in between these two extremes.

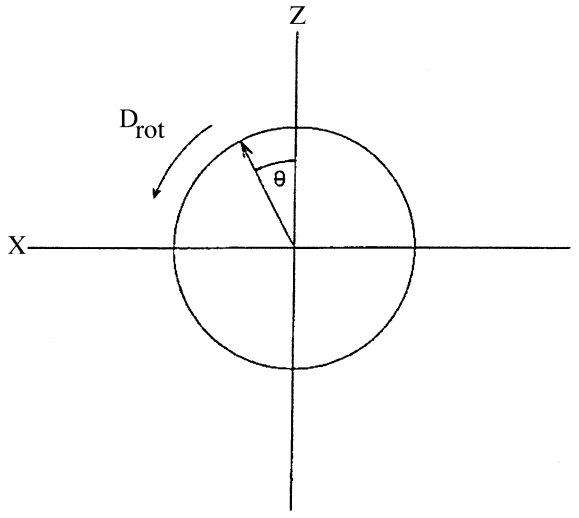

Fig. 4. The figure shows the angular coordinate θ made by the rotating dipole with the z-axis which is the polarization axis of the exciting laser beam.

3.3. Rotational dynamics of $DiIC_{18}(5)$ in egg PC

$DiIC_{18}(5)$ is a linear chromophore attached with two octadecyl chains. This dye is insoluble in water and it is easily solubilized in bilayer vesicle

membranes of egg PC. By virtue of the structure, the chromophore lies on the surface of the membrane [30,31]. The fluorescence decay is biexponential with lifetimes (amplitudes) 1.29 ns (0.36) and 0.39 ns (0.64). The lifetime values are unchanged upon a four-fold dilution. Both the lifetimes are therefore associated with the monomer of the dye. The translational diffusion coefficient of the lipid in the membrane is typically of the order of 10^{-12} m^2 s^{-1}, which is also the value for most molecules of comparable molecular weight [32]. The diffusion length in two dimensions $[\langle r^2 \rangle^{1/2} = 2(D_{tr}\tau_f)^{1/2}]$ of the dye during the lifetime of the excited state is 0.7 Å which is far less than the diameter of the sonicated vesicle (≈ 300 Å) or giant liposome (≈ 10 μm). Therefore, the contribution due to the translational diffusion on the curved surface of the membrane for the fluorescence depolarization during the excited state lifetime of the dye may be neglected. The fluorescence depolarization is essentially determined by the wobbling/rotational dynamics of the dye on the plane of the membrane.

The fluorescence anisotropy decay of $DiIC_{18}(5)$ solubilized in a single giant liposome obtained by fluorescence microscopy is shown in Fig. 5. Theory and the Monte Carlo simulation predicts that the anisotropy decay for this case should be single exponential:

$$\frac{r(t)}{r(0)} = \exp(-4D_{rot}t) \tag{13}$$

where D_{rot} is the rotational diffusion constant on the surface of the membrane. Experimentally measured fluorescence anisotropy decay is consistent with this. The experimental data is fitted to Eq. (13) and the value of D_{rot} is obtained as $D_{rot} = 1.56 \times 10^8$ s^{-1}. More importantly, the anisotropy decays to zero as expected from the Monte Carlo simulations and the theory. The systematic deviation of experimental points below 1 ns from the trend line in Fig. 5 may be due to some of the fast dynamics which are not taken into account in this model.

The fluorescence anisotropy decay of $DiIC_{18}(5)$ solubilized in sonicated vesicles was obtained for the sample in a cuvette. The typical size of these

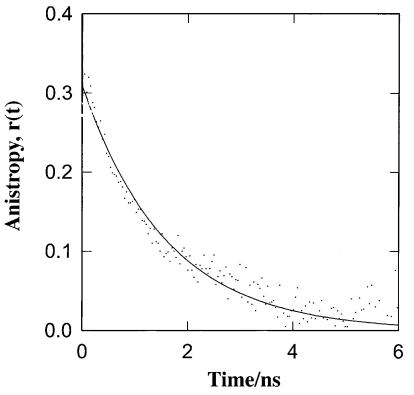

Fig. 5. Fluorescence anisotropy decay of $DiIC_{18}(5)$ in a single giant liposome. The concentration ratio was $DiIC_{18}(5)$/[lipid] = 1:118. The decay was collected at the excitation wavelength of 600 nm and the emission over 645 nm at 25°C. The smooth line is the best fit of $r(t)$ to an exponential function [Eq. (13)].

vesicles is approximately 300 Å [20]. In this case, the fluorescence anisotropy is the average measured over several vesicles (Fig. 1). Fig. 6 shows the anisotropy decay. Unlike the single liposome experiment, the anisotropy does not decay to zero. This agrees with the prediction from Monte Carlo simulations and theoretical equations. As described earlier, the anisotropy decay for this case

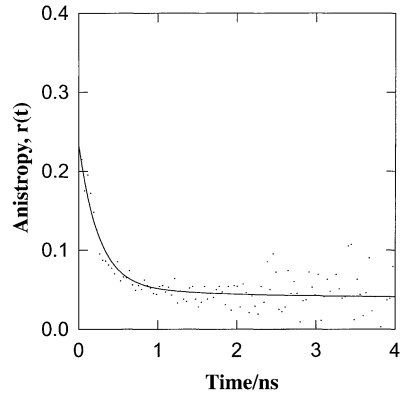

Fig. 6. Fluorescence anisotropy decay of $DiIC_{18}(5)$ in sonicated vesicles. The concentrations used were $[DiIC_{18}(5)] = 0.80$ μM and [lipid] = 0.14 mM. The decay was collected at the emission wavelength 670 nm with the excitation wavelength of 600 nm at 25°C. The smooth line is the best fit of $r(t)$ to Eq. (15). See text for the values of best fit parameters.

should be a single exponential with a constant term:

$$\frac{r(t)}{r(0)} = \tfrac{3}{4}\exp(-4D_{rot}t) + \tfrac{1}{4} \quad (14)$$

The rotational dynamics of the molecule on the surface is expected to be identical for the giant liposome and sonicated vesicles and hence D_{rot} to be nearly same. The best fit of the anisotropy decay to Eq. (14) shows that the data is poorly fitted. The misfit is due to a fast depolarization component. The experimental data were then fitted to Eq. (15), as shown in Fig. 6, containing a fast relaxation term in addition to the rotational diffusion term $(\tau_r = 4D_{rot})^{-1}$ term:

$$\frac{r(t)}{r(0)} = p + q\exp(-4D_{rot}t) + r\exp\left(-\frac{t}{\tau_{fast}}\right) \quad (15)$$

The best fit parameters are $p = 0.17$, $q = 0.08$, $r = 0.75$, $\tau_{fast} = 0.18$ ns with D_{rot} fixed at 1.56×10^8 s^{-1}. Considering the molecular length (≈ 16 Å) as the radius of the circle on which the dipole is rotating, the diffusion coefficient D on the surface was calculated as 4.01×10^{-10} m^2 s^{-1}.

The observed fast relaxation time of $\tau_{fast} = 0.18$ ns is not due to scattered light from the vesicles. The scattering intensity ($\lambda_{ex} = 600$ nm) was negligible at the emission wavelength $\lambda_{em} = 670$ nm because of the 645 nm cut-off filter used. Considering the structure of the dye and its anchoring on the surface of the membrane, the molecule has the freedom to wobble in a cylinder of volume $\pi R^2 l$ [l is the length of the dye molecule which is the length of the cylinder and R is the radius of the cylinder (mean displacement of the dye)] about the surface of the membrane, apart from the rotational diffusion (D_{rot}) on the surface. The wobbling-in-cylinder dynamics is the surface equivalent to the wobbling-in-cone model [6,7] for a linear dye molecule which is intercalated inside the membrane. Therefore, we attribute this fast relaxation to the wobbling-in-cylinder dynamics of $DiIC_{18}(5)$. Fig. 7 illustrates the proposed model of wobbling-in-a-cylinder dynamics for the surface dynamics of $DiIC_{18}(5)$.

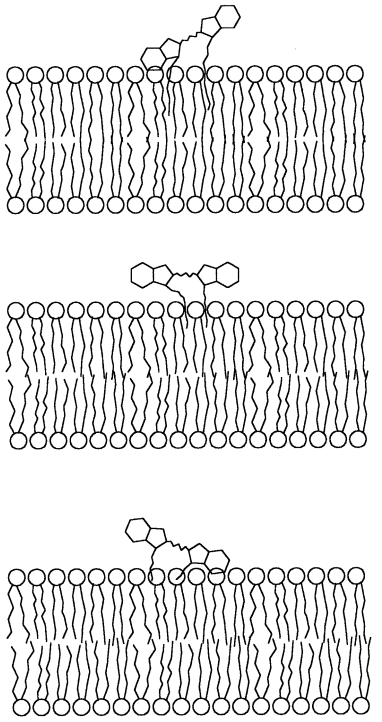

Fig. 7. Proposed wobbling-in-a-cylinder model for the surface dynamics of $DiIC_{18}(5)$. Three representative orientations of the dye on the surface of the membrane are shown.

The fluorescence anisotropy experiments were also carried out on $DiIC_{18}(5)$ in egg PC sonicated liposomes prepared in buffers of different pH to characterize this fast relaxation component. The values of τ_{fast} (Eq. (15)) obtained from the best fits to the experimental data were 0.31, 0.18 and 0.36 ns at the pH values 4.0, 7.0 and 9.0, respectively. The variation of the pH is known to affect the packing of lipid molecules and consequently the dynamics [33,34]. This effect will be larger in the head group region which contains polar groups compared to the hydrophobic tail region. The strong dependence of the fast rotational correlation time with the pH supports the argument that the process causing this fast depolarization is the one associated with the surface of the membrane. This fast anisotropy component was also observed in the case of other lipids such as DMPC (C14:0,

1,2-dimyristoyl phosphatidyl choline) and DPPC (C16:0, 1,2-dipalmitoyl phosphatidyl choline) and is of the same order (0.18 ± 0.05 ns). In the case of egg PC vesicles prepared in sucrose solutions, this fast correlation time increases from 0.18 to 0.27 ns with the increase of sucrose concentration from 0 to 44.4% w/w, supporting the argument that the process associated with this fast relaxation is the one that can be associated with the surface of the membrane. The slow correlation time due to the rotational diffusion on the surface also increases from 1.60 to 2.78 ns with the increase of sucrose concentration in the aqueous medium.

Therefore, in the case of the surface probe $DiIC_{18}(5)$ in egg PC vesicles, two depolarizing motions contribute to the fluorescence anisotropy decay: rotational diffusion on the membrane surface (1.60 ns); and wobbling-in-a-cylinder dynamics about the membrane surface (0.18 ns).

It may be noted that the fast relaxation was not observed in the depolarization dynamics of $DiIC_{18}(5)$ in single giant liposomes. This is understood as follows. In single giant liposomes, the fluorescence depolarization is measured in two dimensions (on the surface of the membrane). In this case, rotational motion on the surface depolarizes the fluorescence whereas the wobbling-in-cylinder dynamics does not depolarize the fluorescence as this dynamics is in the direction that is perpendicular to the plane of observation.

It is a common practice in literature to apply the same mathematical models to interpret the fluorescence anisotropy decays of fluorescent probes in highly curved surfaces such as membranes, whether the observation is made using the fluorescence microscopy or in normal cuvette experiments. However, this study points out the fact that although the dynamics of the probe is similar in both the cases illustrated here, the way the anisotropy is measured in the observation volume can lead to different results based on the way the information is averaged over the surface. Sometimes, this can result in misinterpretation of the fluorescence anisotropy data. For example, the value of r_∞/r_0 that can be directly determined from the anisotropy decay curve, can not be treated as an indication of the dynamical freedom of the probe and as a model/technique independent parameter. In the two cases illustarted here, although the probe is experiencing similar dynamics, the value of r_∞/r_0 in the case of a plane is 0 whereas, in the case of a sphere, it is 0.25.

4. Summary

The rotational diffusion of dye probes on the surface of a sphere was simulated using Monte Carlo procedures and compared with the theoretical equations. The anisotropy does not decay to zero in the case of rotational diffusion of dipoles on the surface of the sphere whereas it decays to zero in the case of rotational diffusion on a plane. That means, the limiting value of the anisotropy depends on the geometry of the surface on which the dipoles are undergoing rotational diffusion. The decay time in both cases is $(4D_{rot})^{-1}$ where D_{rot} is the rotational diffusion coefficient. The agreement between the Monte Carlo simulations and the theoretical equations justify the applicability of the simulation methods to the case of diffusion on more complicated curved surfaces that can not be treated analytically. The solutions obtained for rotational diffusion equations were applied to the interpretation of the anisotropy decay of the dye probe $DiIC_{18}(5)$ in small and giant membranes.

Acknowledgements

The authors thank Prof G. Krishnamoorthy for his help with the fluorescence microscopy experiments.

References

[1] J.R. Lakowicz, Principles of Fluorescence Spectroscopy, Plenum Press, New York, 1983.
[2] G.R. Fleming, Chemical Applications of Ultrafast Spectroscopy, Oxford University Press, New York, 1986.
[3] R.F. Steiner, Fluorescence anisotropy: theory and applications, in: J.R. Lakowicz (Ed.), Topics in Fluorescence Spectroscopy, 2, Plenum Press, New York, 1991, p. 1.
[4] W.W. Mantulin, G. Weber, Rotational anisotropy and solvent–fluorophore bonds: an investigation by differ-

ential polarized phase fluoremetry, J. Phys. Chem. 66 (1977) 4092–4099.
[5] R.L. Christensen, R.C. Drake, D. Philips, Time resolved fluorescence anisotropy of perylene, J. Phys. chem. 90 (1986) 5960–5967.
[6] K.J. Kinosita, S. Kawato, A. Ikegami, A theory of fluorescence polarization in membranes, Biophys. J. 20 (1977) 289–305.
[7] G. Lipari, A. Szabo, Effect of librational motion on fluorescence depolarization and nuclear magnetic resonance relaxation in macromolecules and membranes, Biophys. J. 30 (1980) 489–506.
[8] J.M. Beechem, L. Brand, Time-resolved fluorescence of proteins, Annu. Rev. Biochem. 54 (1985) 43–71.
[9] U.K.A. Klein, H.P. Haar, Picosecond time dependent rotational diffusion of rhodamine 6G in micellar solution, Chem. Phys. Lett. 58 (1978) 531–536.
[10] A.J.W.G. Visser, K. Vos, A.V. Hoek, J.S. Santema, Time-resolved fluorescence depolarization of rhodamine B and octadecylrhodamine B in Triton X-100 micelles and aerosol OT reverse micelles, J. Phys. Chem. 92 (1988) 759–765.
[11] E.L. Quitevis, A.H. Marcus, M.D. Fayer, Dynamics of lipophilic probes in micelles: picosecond fluorescence depolarization measurements, J. Phys. Chem. 97 (1993) 5762–5769.
[12] N.C. Maiti, S. Mazumdar, N. Periasamy, Dynamics of porphyrin molecules in micelles. picosecond time-resolved fluorescence anisotropy studies, J. Phys. Chem. 99 (1995) 10708–10715.
[13] N.C. Maiti, M.M.G. Krishna, P.J. Britto, N. Periasamy, Fluorescence dynamics of dye probes in micelles, J. Phys. Chem. B 101 (1997) 11051–11060.
[14] P.W. Kuchel, A.J. Lennon, C. Durrant, Analytical solutions and simulations for spin-echo measurements of diffusion of spins in a sphere with surface and bulk relaxation, J. Magn. Reson. 112 (1996) 1–17.
[15] M.M.G. Krishna, R. Das, N. Periasamy, R. Nityananda, Translational diffusion of fluorescent probes on a sphere: Monte Carlo simulations, theory and fluorescence anisotropy experiment, J. Chem. Phys. 112 (2000) 8502–8514.
[16] M.M.G. Krishna, J. Samuel, S. Sinha, Brownian motion on a sphere: distribution of solid angles, J. Phys. A: Math. Gen. 33 (2000) 5965–5971.
[17] W.H. Press, S.A. Teukolsky, W.T. Vetterling, B.P. Flannery, Numerical Recipes in C: The Art of Scientific Computing, 2nd ed., Cambridge University Press, 1992.
[18] L. Jansen, M. Boon, Theory of finite groups. Application in Physics: Symmetry Groups of Quantum Mechanical Systems, North-Holland Publishing Company, Amsterdam, 1967.
[19] G. Krishnamoorthy, A. Srivastava, Intracellular dynamics seen through time-resolved fluorescence microscopy, Curr. Science 72 (1997) 835–845.
[20] G. Krishnamoorthy, Temperature jump as a new technique to study the kinetics of fast transport of protons across membranes, Biochemistry 25 (1986) 6666–6671.
[21] G. Riquelme, E. Lopez, L.M. Garcia-Segura, J.A. Ferragut, J.M. Gonzalez-Ros, Giant liposomes — a model system in which to obtain patch-clamp recordings of ionic channels, Biochemistry 29 (1990) 11215–11222.
[22] N. Periasamy, S. Doraiswamy, B.G. Maiya, B. Venkataraman, Diffusion controlled reactions: fluorescence quenching of cationic dyes by charged quenchers, J. Chem. Phys. 88 (1988) 1638–1651.
[23] K.V. Bankar, V.R. Bhagat, R. Das et al., Techniques for the study of fast chemical processes with half-times of the order of microseconds or less, Indian J. Pure Appl. Chem. 27 (1989) 416–428.
[24] A. Srivastava, G. Krishnamoorthy, Time-resolved fluorescence microscopy could correct for probe binding while estimating intracellular pH, Anal. Biochem. 249 (1997) 140–146.
[25] A. Srivastava, G. Krishnamoorthy, Cell type and spatial location dependence of cytoplasmic viscosity measured by time-resolved fluorescence microscopy, Arch. Biochem. Biophys. 340 (1997) 159–167.
[26] A. Grinvald, I.Z. Steinberg, On the analysis of fluorescence decay kinetics by the method of least-squares, Anal. Biochem. 59 (1974) 583–598.
[27] P.R. Bevington, D.K. Robinson, Data Reduction and Error Analysis for the Physical Sciences, 2nd ed., McGraw-Hill Inc, New York, 1994.
[28] J.R. Knutson, J.M. Beechem, L. Brand, Simultaneous analysis of multiple fluorescence decay curves: a global approach, Chem. Phys. Lett. 102 (1983) 501–507.
[29] A. Abragam, The Principles of Nuclear Magnetism, Oxford University Press, London, 1961.
[30] D. Axelrod, Carbocyanine dye orientation in red cell membrane studied by microscopic fluorescence polarization, Biophys. J. 26 (1979) 557–573.
[31] M.M.G. Krishna, N. Periasamy, Fluorescence of organic dyes in lipid membranes: Site of solubilization and effects of viscosity and refractive index on lifetimes, J. Fluoresc. 8 (1998) 81–91.
[32] A.M. Kleinfeld, P. Dragsten, R.D. Klausner, W.J. Pjura, E.D. Matayoshi, The lack of relationship between fluorescence polarization and lateral diffusion in biological membranes, Biochim. Biophys. Acta 649 (1981) 471–480.
[33] J. Cerbon, The influence of pH and temperature on the limited rotational freedom of the structured water and lipid hydrocarbon chains of natural membranes, Biochim. Biophys. Acta 211 (1970) 389–395.
[34] S. Massari, E. Folena, V. Ambrosin, G. Schiavo, R. Colonna, pH-dependent lipid packing, membrane-permeability and fusion in phosphatidylcholine vesicles, Biochim. Biophys. Acta 1067 (1991) 131–138.